Foam-Assisted Enhanced Oil Recovery: Bridging the Gap between Theory and Practice

Jinesh Machale[1], *Dorcas Annung* Akrong[1], *Omid* Mohammadzadeh[1], *Ali* Telmadarreie[2], *Anand* Yethiraj[3], *Lesley Anne* James[1*]

[1]Department of Process Engineering, Faculty of Engineering and Applied Science, Memorial University of Newfoundland, St. John's, NL A1C 5S7, Canada
[2]Cnergreen Corporation, Life Sciences Innovation Hub (LSIH) 3655 36 St NW, Calgary, AB T2L 1Y8, Canada
[3]Department of Physics and Physical Oceanography, Memorial University of Newfoundland, St. John's, NL A1B 3X7, Canada

Abstract. The utilization of foam in enhanced oil recovery (EOR) applications has been the subject of extensive scientific investigations in last two decades. This is due to its ability to regulate the mobility of residual oil and improve the interfacial properties simultaneously. As a result, foam declines the gas relative permeability and improves overall sweep efficiency. The effectiveness of the foam in EOR application is a function of porosity, permeability, the flow rate of gaseous and liquid phases, capillary pressure, temperature, and salinity. Despite the various benefits associated with foam-assisted EOR, significant challenges have been identified in its implementation. In reservoir-like conditions, foam is susceptible to drying out because the lamella cannot withstand the prevalent capillary pressure resulting from the insufficient liquid. This results in the coalescence and drying of foam. The effectiveness of foam diminishes when it dries out, leaving only the liquid phase, thereby causing the relative permeability to resemble that of water injection. The present study suggests a best practise workflow to address the aforementioned issues in foam-assisted EOR (theoretical, experimental, and simulation perspectives). The workflow consists of characterizing the foam independently before conducting an optimized coreflood. We purport that more thought into the form of the semi-empirical local equilibrium (LE) model may be warranted. Furthermore, the study provides a workflow to gain valuable insights to improve the effectiveness of foam-assisted EOR application.

1 Introduction

Due to the inadequate ability of the renewable energy sector to fulfil vast worldwide energy demands, it is anticipated that, at least in the near future, the world will continue to heavily rely on fossil fuels. Primary (i.e., natural lift) and secondary (i.e., waterflooding) recovery methods can retrieve about 10–30 % of the original oil in place from most conventional oil reservoirs. Tertiary oil recovery methods, also known as enhanced oil recovery (EOR) processes, are designed to produce higher percentages of the remaining oil in place after expiry of the primary and secondary recovery methods [1–3]. Steam, gas, and chemicals injections are frequently used in the EOR methods to mitigate capillary forces, increase remaining oil mobility, and alter the interfacial characteristics between the oil and water [2,4,5]. However, there are certain challenges associated with these injection methods such as viscous fingering, retention and stability of chemical additives at reservoir conditions, and premature gas breakthrough [6]. For the past two decades, researchers have been extensively considering the application of foam in EOR processes [7–9]. Typically, foam refers to a dispersion of a non-wetting gaseous phase within a continuous wetting liquid phase [10,11]. Foam meritoriously regulates the mobility ratio by decreasing the displacing phase mobility (through increasing apparent viscosity of the injecting phase) and enhances the micro- and macroscopic displacement efficiency by reducing the interfacial tension (IFT) between oil and water, and redirecting flow of the injecting phase toward low permeability zones [12]. Chemical additives (essentially surfactant) are commonly used to reduce the IFT between oil and water during adsorption at the oil–water interface. This phenomenon results in the breakup of trapped oil into smaller droplets at pore throats, facilitating its passage through pores of rock for additional oil recovery [13]. Interactions between foam and oil occur at the displacement front, and depending on factors like crude oil composition, entrance coefficient, and spreading coefficient, the foam may initially coalesce into substantial gas slugs [14,15]. This coalescence is influenced by the formation of an uneven oil-water-gas film, which affects the capillary pressure [16]. The distribution of fluids within porous media is primarily influenced by the wettability of the media [8,17,18]. As foam flooding progresses, surfactant molecules cover the oil-wet rock surface, reducing its interaction with oil and causing a shift from oil-wet to water-wet conditions. This change in wettability enhances foam stability. Moreover, the foam bank zone promotes the formation of smaller bubbles, contributing to the overall effectiveness of the process.

Despite these clear advantages, there are several significant drawbacks associated with foam-assisted EOR. These mainly include operational issues (i.e., excessive injection pressure and unstably maintained flow rates due to high viscosity) and foam quality issues (i.e., potential foam collapse upon contact with oil as well as dry-out events) [19,20]. In a

* Corresponding author: ljames@mun.ca

recent series of lab-scale coreflooding experiments, we observed that the lamella, a constituent of the foam structure, suddenly collapsed, and the unstable foam did not withstand the prevailing capillary pressure, which resulted in foam dissociation, liquid phase dominance in the displacing fluid, and incomplete sweep of the low permeability regions [21]. The relative permeability characteristics of such system resembles a waterflooding scenario, which ultimately undermined the overall oil recovery process. Very little literature on foam-assisted EOR adequately addresses critical aspects of the process, focusing on, the interaction(s) between foam chemical additives, reservoir rock, and polar components of the crude oil. Moreover, a thorough understanding of how foam film deforms under shear and how temperature and pressure affect foam stability are often neglected. These factors are essential for achieving efficient displacement and optimal foam performance in oil recovery [22,23]. The present study systematically addresses the aforementioned issues by elucidating the role of adsorption of chemical additives, associated with foam on both rock and oil surfaces, foam mobility parameters (i.e., apparent viscosity, viscoelasticity, foam quality, relative permeability, and mobility reduction factor), pressure and temperature on the production performance of foam-assisted EOR. The present study also extensively describes the empirical foam model implemented in a commercial reservoir simulator (CMG–STARS®) in terms of its significance, agreement with experimental data, and overall performance.

2 Foam-assisted EOR

2.1 Foam structure and its flow through porous media

The foam structure is a function of the amount of liquid and gas. When there is a substantial amount of liquid in the foam, it is commonly known as *kugelschaum* or wet foam (usually spherical in shape). Otherwise, it is known as *polyederschaum* or dry foam (polyhedral in shape) (Fig. 1 (a)) [11]. Typical foam structure can be classified into three parts; *viz.* lamella, Plateau border, and node (Fig. 1 (b)). Usually, the lamella is a thin 2D liquid film, and the films meet in threes at a Plateau border. Nodes, on the other hand, represent the specific locations where at least four Plateau borders intersect. Foam is thermodynamically unstable and its stability is the critical factor for a successful oil recovery process [10]. Studies confirmed that numerous chemical additives (i.e., surfactant, polymer, nanoparticles, and alkali) are excellent foam stabilizers [8]. These chemical additives aid the formation of a robust and uniform film, which eventually impedes the coalescence of foam bubbles meaning more stable foam. We discuss the role of aforementioned chemical additives in foam stability in detail in Section 2.2.

The Marangoni effect, film elasticity, and intermolecular and surface forces are important to comprehend foam stability [24]. Surfactant molecules move towards the boundaries of the foam film as it drains, a phenomenon known as the *Marangoni effect*. This effect prevents abrupt surface contractions and expansions, which aids in stabilizing thin foam layers [11]. An insight into the surface and intermolecular forces is beneficial due to their impact on the foam stability. The disjoining pressure, explained by the DLVO theory, illustrates the attracting (also known as the van der Waals) and repulsive (commonly referred to as an electrostatic double layer) forces between interfaces in the thin foam film [25]. Ionic chemicals that have been adsorbed at the interfaces cause electrical charges, which create a repulsive force that improves foam stability. Film rupture, on the other hand, is facilitated by the attractive van der Waals force. The total disjoining pressure in the foam film, as determined by the DLVO theory, is determined by the sum of these forces, with a repulsive energy barrier preventing film rupture. The foam film ruptures due to the attraction force when this energy barrier is overcome [26]. Furthermore, foam film elasticity, influenced by surface area and surface tension, determines the film's ability to self-heal after external damage [27].

For effective implementation, it is crucial to comprehend foam properties, how it is generated, and how it behaves in porous media. Foam flow in porous media is distinguished into three regimes, *viz.* continuous gaseous phase, trapped (or immobile) bubble, and mobile foam regimes [28]. Lamella or bubble division, snap-off, and leave-behind are fundamental mechanisms that cause the foam to form in porous media (Fig. 1(c)) [29,30]. As foam flows through porous media, a portion of the overall non-wetting gas saturation exists as the flowing gas. This may appear either in a continuous or discontinuous manner. Simultaneously, the remaining gas becomes trapped within the porous media, forming an intermittent or disjointed phase. The presence of foam bubbles within the pore network of rocks can manifest in both trapped and flowing phases. Therefore, the amount of gas that becomes trapped assumes a vital role in determining the efficacy of foam propagation in porous media. In contrast, the liquid wetting phase is continuous and moves through narrow pores, while the continuous gas and foam occupy medium and large pores [29]. In sum, the foam flow in the porous media is proportional to factors like the rate of foam generation, the strength (strong or weak), and the stability of the foam at the pore scale under reservoir conditions [31].

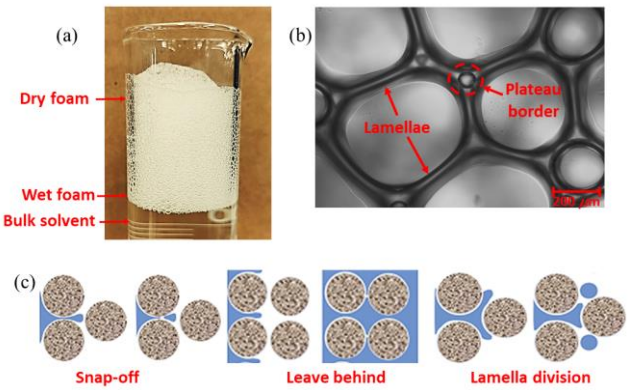

Fig. 1. Illustration of (a) wet and dry foam and (b) typical foam structure [Material: 0.25 wt. % sodium dodecyl sulphate solution (an anionic surfactant, typically used in EOR application)], and (c) principal mechanisms of foam generation at the pore-scale.

2.2 Stability of foam

The most critical component of foam-assisted EOR is its stability. This section highlights vital parameters for controlling foam stability in porous media, such as the association of

chemical additives, foam injection design, experimental conditions, interfacial properties, and petrophysical properties of rock [32]. Foam stabilizer commonly uses a number of chemical additions, including surfactant, alkali, nanoparticles, polymers, and their combinations [8,33]. Typical surfactants are organic compounds with at least a hydrophobic (referred to as tail and are oil-soluble) and a hydrophilic (referred to as the head, are water-soluble, and can be ionic or nonionic) groups in their molecule. This specific molecular structure causes the hydrophilic component to adsorb at the interface (gas–water and oil–water), which reduces the interfacial forces and free energy at these interfaces [34,35]. Surfactant adsorption in foam films occurs in two steps: First, surfactant molecules adsorb from the sub-layer region to the film's surface. Initially, adsorption happens in Plateau borders and lamellae. The second-step involves the irreversible movement of surfactant molecules from the bulk solution to the surface through diffusion, possibly with convection (Fig. 2) [36]. Surfactant diffusion spans a much larger domain than the adsorption layer's thickness.

There are several commonly practiced surfactants introduced in the literature that could be used as foam stabilizers due to their excellent foamability, strength to salinity, and wide range of temperature and pH resistance, categorized into anionic (alfa olefin sulfonate, sodium dodecyl sulfate, internal olefin sulfonates, etc.), cationic (cetyltrimethylammonium bromide and hexadecyltrimethylammonium bromide), nonionic (Brij 35 and Tween 80), and zwitterionic (Lauryl betaine, N-dodecyl-N, N-dimethyl-3-ammonio-1-propanesulfonate, and cocamidopropyl betaine) [32,37–40].

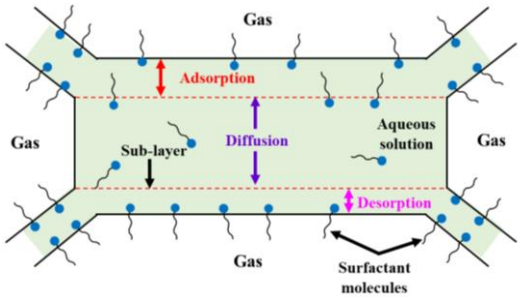

Fig. 2. A 2-dimensional illustration of the adsorption mechanism in the lamellae during foam generation.

Polymers can also be utilized in the foam-assisted EOR applications owing to their efficient mobility control, foam stabilizing characteristics, and compatibility with oil. Polymers reduce coalescence and surfactant desorption from the foam film [41]. Biodegradable synthetic polymers (polyacrylamide and partially hydrolyzed polyacrylamide) and polysaccharides (xanthan gum and guar gum) are often used as foam stabilizers because of their high tolerance to shear, salt and temperature [42,43].

2.3 Challenges associated with foam-assisted EOR

In our earlier work, we extensively studied the performance of a novel nanoparticles-based foam (ArmorFoam) using interfacial and core flooding analyses [21]. In comparison with baseline waterflooding scenario, a significant 13.2–24 % additional oil was recovered by injecting different sequences of ArmorFoam, nitrogen gas, and brine solution. However, we observed pressure difference (ΔP) abnormalities; likely due to foam coalescence and excess foam dry-out at the end of core flooding experiments. In order to gain a comprehensive understanding of how ArmorFoam works in increasing the oil recovery, we return to the basic principles of colloids and interface science. This includes examining the adsorption of ArmorFoam at gas–water and oil–water interfaces. Additionally, it is important to investigate mass transfer phenomena, such as the gas diffusion into the aqueous phase and the adsorption of chemical additives onto rock surfaces. Lastly, studying the foam deformation by shear is another integral part of the fundamental approach that will likely provide clarity on abnormalities observed during the preliminary experiments. In Sections 3 and 4, we discuss a systematic methodology developed for efficient characterization of foam as well as optimization of the foam-assisted EOR process. Additionally, we include our recommendations to enhance the effectiveness of this EOR process in the context of a robust characterization and evaluation workflow.

3 Foam characterization and optimization techniques-EOR application

Even though the bulk-phase foam differs from the foam generated in porous media, their fundamental properties remain the same. *In-situ* foam generation, flow through porous media, and its performance in terms of increased oil recovery can be assessed using coreflooding experiments. However, it is essential to characterize bulk foam to optimize the concentration of chemical additives and determine its physicochemical properties. This section is dedicated to introduce foam characterization methods at bulk scale as well as when porous media surfaces are involved. Fig. 3 demonstrates the recommended sequence of actions to ensure the effective implementation of foam-assisted EOR. Although it is challenging to establish a comprehensively prioritized step due to the variations in the system, we strongly advise focusing on characterizing chemical additives, rock, and crude oil as a primary step. Further, conducting adsorption, interfacial, and rheological analyses to study their interactions is highly recommended. These experiments will enhance our understanding of the materials and their mutual interactions. Once we have gained insights into these interactions, investigating foam flow through porous media is suggested.

3.1 Foamability

Foam is typically defined by its foamability. It refers to the capacity of a surface-active agent solution to generate foam and is quantitatively evaluated based on the initial foam volume or height, measured shortly after foam generation (see Fig. 4) [44,45]. Generally, bulk foam can be formed by simply shaking and intensely stirring (ASTM D3519-88) the surface-active agent solution. Several studies extensively examined the foamability of various surface-active agents under high-temperature and high-pressure conditions [46,47].

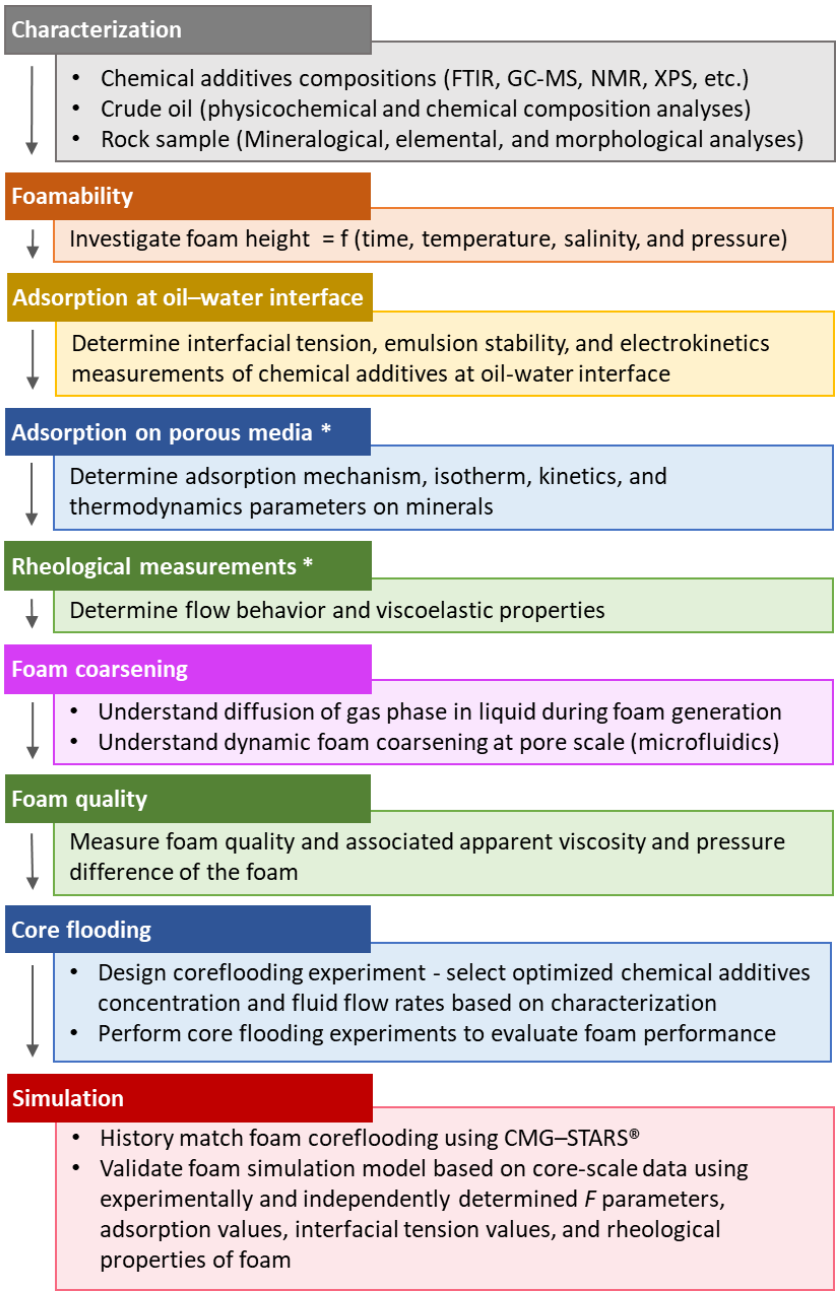

Fig. 3. Recommended workflow to assess foam-assisted EOR. (*investigations conducted in the present study).

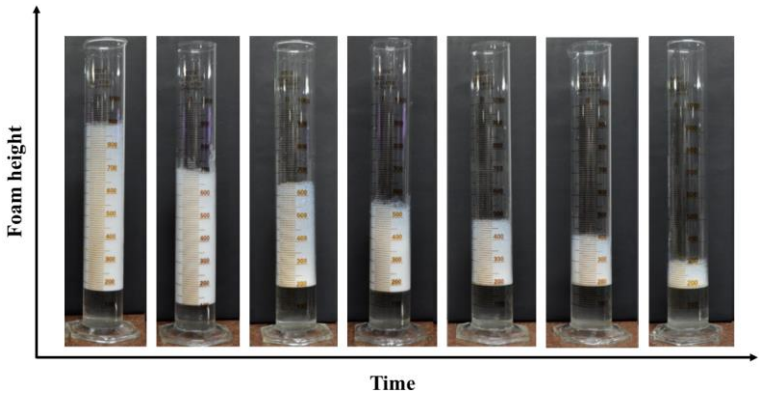

Fig. 4. Variation in the foam height with respect to time [Material: 0.25 wt. % sodium dodecyl sulphate].

3.2 Adsorption of chemical additives at oil–water interface

The performance of a surfactant used in foam-assisted EOR is directly dependent on its ability to generate foam and to reduce IFT between crude oil and water. This interfacial phenomenon is associated with the adsorption of the surfactant at the oil–water interface and thus the need to understand and quantify adsorption of surfactant at the oil–water interface. Note that the discussions provided in this section only focus on an immiscible fluid system, composed of oil and water, and that only surfactants soluble in the aqueous phase are considered. Surfactant adsorption at the oil–water interface is primarily governed by the concentration of surfactant in the aqueous phase [11]. The IFT reduces with increasing surfactant concentration and reaches a minimum at the critical micelle concentration (CMC). Generally, below the CMC, the IFT reduces rapidly with the surfactant concentration due to the presence of vacant sites at the interface. At the CMC, a monolayer of the surfactant molecules is formed on the interface, and hence the IFT becomes constant. When the surfactant concentration increased above CMC, the change in IFT is rather small (see Fig. 5(a)) [48]. The accuracy of the IF data can be verified by calculating the surface excess concentration through the application of the Gibbs adsorption isotherm (see Equation 1) [49].

$$\Gamma = -\frac{1}{2RT}\frac{d\gamma}{d\ln c} \quad (1)$$

the universal gas constant (J mol^{-1} K^{-1}), γ is the interfacial tension (N m^{-1}), T is the temperature (K), and c is the surfactant concentration (mol m^{-3}). To assess a surfactant's performance in IFT reduction, the measurements should be performed at real reservoir operating conditions and fluid composition/salinity. It is not advisable to conduct these measurements in ambient aerobic conditions, as the presence of air can significantly alter the interfacial properties of the liquid [50]. Adsorption of chemical additives can be studied at three scales, *viz*. macroscopic, mesoscopic, and microscopic (see Fig. 5(b)). Knowledge of the macroscopic scale is required to understand the efficacy of chemical additives and their interaction with crude oil [51]. Mainly, it includes the phase behavior studies, which determines the discrete volumes of oil, water and water/oil mixture in the presence of chemical additives. The mesoscopic scale can reflect coalescence, flocculation, and sedimentation of a dispersed phase better. Further, the microscopic scale is utilized to investigate the development of a film at the oil–water interface [52]. Microscopically, zeta potential, conductivity, nuclear magnetic resonance, UV-vis spectroscopy, small-angle X-ray scattering, and dynamic light scattering are some of the analyses used for understanding the adsorption chemical additives on the oil–water interface [11,49].

Readers are also recommended to systematically characterize the oil sample's physicochemical properties (such as density, viscosity, acid number, base number, and API gravity) and chemical composition (such as asphaltenes, wax, and sulfur). This will ensure an understanding of the chemical interaction and adsorption mechanism of chemical additives at the oil–water interface.

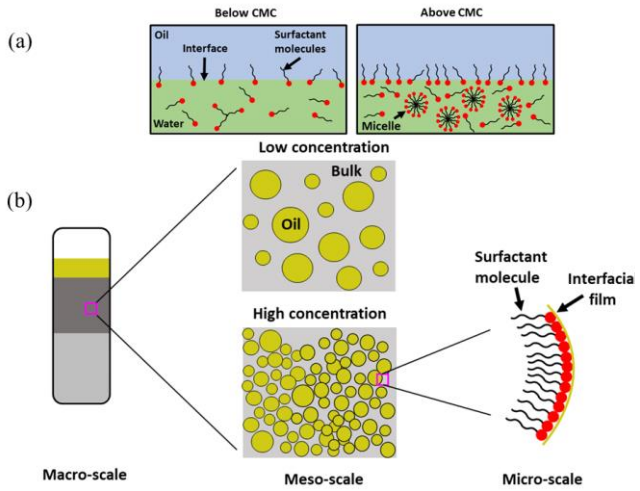

Fig. 5. (a) Mechanism of the adsorption of the surfactant molecules at the oil–water interface and (b) adsorption occurring on a multiscale level.

3.3 Adsorption of chemical additives on the porous media

Surfactants are considered effective chemical additives in EOR applications because of their capacity to achieve extremely low IFT between crude oil and water and to change the wettability of reservoir rock (primarily oil- to water-wet). The possible loss of surfactant molecules due to their adsorption on the pore surfaces of the porous media is a serious issue when employing surfactants in oil recovery applications [53,54]. Therefore, it is essential to perform adsorption experiments (both static and dynamic) to analyze the adsorption kinetics, mechanism, and thermodynamics [55,56]. The adsorption mechanism of surfactant on the rock surface can be evaluated with the help of numerous isotherm models [such as Langmuir (monolayer adsorption), Freundlich (adsorption on the heterogeneous surfaces), Temkin (impact of interaction on overall adsorption), Redlich-Peterson (includes fundamental of both Langmuir and Freundlich), etc.]. Moreover, the kinetics of adsorption characterized by equilibrium adsorption capacity (q_e) and rate constant of adsorption (k) with the pseudo-first-order, pseudo-second-order, and intraparticle diffusion models. The readers are recommended to refer to the review article by Belhaj et al. [57] where they have systematically described the impact of concentration of surfactant, pH, salt, minerals, and temperature on the adsorption of numerous types of surfactants on the rock surface. In addition, the experimental steps for adsorption measurement were thoroughly discussed.

Adsorption of ArmorFoam on the crushed Berea sandstone surfaces (mesh size: 60–80 and surface area: 3.90 ± 0.20 m^2 g^{-1}) at varying ArmorFoam concentrations was studied, and the results are shown in Fig. 6 and Table 1. It is evident from Fig. 6 that with increasing concentration, the amount of adsorption (q_e) increases. This phenomenon can be attributed primarily to the combined effects of electrostatic forces and chemical interactions between the surface-active components of ArmorFoam and the Berea sandstone surface [58]. The Langmuir adsorption isotherm effectively illustrated the adsorption process (see Table 1). The adsorption rate of ArmorFoam on Berea sandstone was determined to be as low as 5%, which is significantly lower compared to the conventionally used surfactants in EOR applications. This indicates that the

loss of surface-active components in ArmorFoam is nominal, making it highly suitable for efficient oil recovery. The reduced adsorption can be primarily attributed to incorporating nanoparticles.

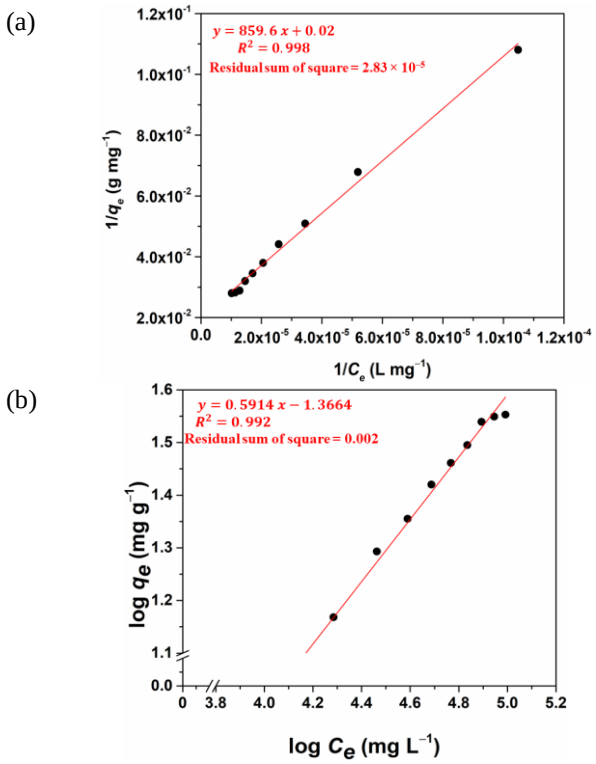

Fig. 6. Variation of equilibrium adsorption of ArmorFoam on sandstone surfaces at different initial concentrations, fitted with (a) Langmuir and (b) Freundlich adsorption isotherms.

3.4 Rheological properties of bulk foam

The study of fluids deformation (primarily liquids and viscoelastic) under the applied force is called *rheology* [59]. Knowledge of the rheology of chemical additives (such as surfactant, polymer, nanoparticles, etc.) solutions and foam used in EOR at reservoir conditions is essential to understand the foam stability, selection of chemicals and their retention in porous media, estimation of the mobility of injection slug, and for the efficient design of flooding [2]. The flow behavior (primarily the viscosity) of fluid can be determined by rheometer at applied shear. Furthermore, the viscoelastic nature (i.e., material with both viscous and elastic behavior) of viscoelastic fluids and foam (essentially, when nanoparticles and polymers are involved) can be well demonstrated by amplitude and frequency sweep tests. Generally, the storage modulus (G') and loss modulus (G'') demonstrate the viscoelastic solid-like and liquid-like behavior, respectively. The G' and G'' are used to measure the amount of energy accumulated and released in sample under oscillatory stress [8,59].

Fig. 7(a) shows the apparent viscosity of ArmorFoam as a function of shear rate (i.e., 0.01–10 s^{-1}) and temperature (25–60°C). The experiments were conducted utilizing an MCR 301 rheometer (make: Anton Paar), employing a parallel plate geometry with a diameter of 50 mm. As shown in Fig. 7(a), apparent viscosity of ArmorFoam decreased by an increase in the shear rate. This phenomenon can be attributed to the deformation and rupturing of the foam film, which commonly reduces bulk foam viscosity under higher applied shear conditions [60]. The viscoelastic properties of ArmorFoam can be observed from Fig. 7 (b and c). To identify the linear viscoelastic (LVE) region, an amplitude sweep test was conducted, maintaining a constant frequency of 1 Hz and subjecting the material to a strain range of 0.01–100% (see Fig. 7(b)). This region allows for conducting tests on the sample without causing any structural damage [61]. Furthermore, the frequency sweep test revealed the $G' > G''$ (see Fig. 7(c)), indicating the viscoelastic-solid features within the sample's LVE region. The presence of a dominant G' in foam films ensures their resistance to deformation, consequently contributing to the overall stability of the foam structure [62].

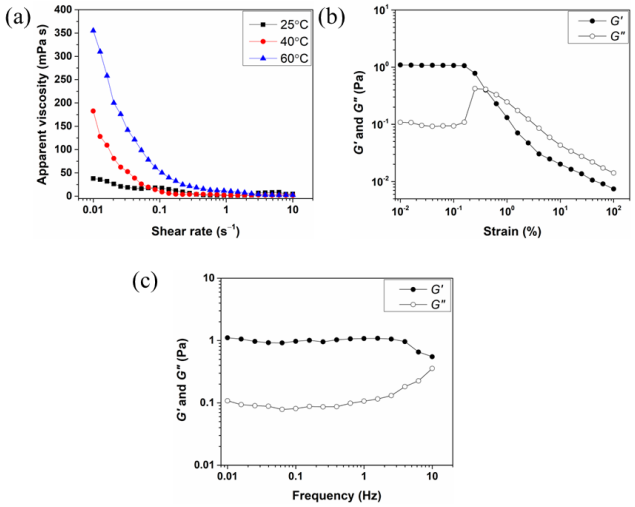

Fig. 7. Rheological properties of ArmorFoam: (a) apparent viscosity, (b) amplitude sweep, and (c) frequency sweep.

3.5 Foam coarsening in porous media

Foam coarsening in porous media is a diffusion phenomenon (also known as Ostwald ripening), where the foam bubbles expand due to the consumption of smaller bubbles by the larger ones over time, eventually reducing the foam's stability and effectiveness (see Fig 8(a)) [63]. As discussed in Section 1, foam reduces the gaseous phases' viscous fingering and premature breakthrough; and maintains the steady displacement front. However, the performance of foam relies on its stability under harsh reservoir conditions. Foam coarsening in the porous media is not fully understood yet. In general, foam bubbles quickly grow to be the same size as or larger than the pore bodies, and thin lamellae can disperse gas considerably more quickly than bulk solvent or Plateau borders. Moreover, lamellae also move and foam bubbles reconstruct to obtain their smallest interfacial energy (see Fig 8(b)) [64].

The rate of foam coarsening in porous media is a function of the foam texture, gas solubility and diffusivity, surfactant, an association of chemical additives, and petrophysical properties of rock [65]. The network of Plateau borders and water zones (i.e., accumulation of water within the pores due to a strong capillary force) influences the flow behavior of foam within porous media during coarsening. While water zones have narrower apertures compared to Plateau borders, they exhibit larger areas. The differences in

Table 1. Adsorption isotherm parameters

Isotherm	Formula	Isotherm parameters		
Langmuir	$\frac{1}{q_e} = \frac{1}{q_0 K_l C_e} + \frac{1}{q_0}$	K_l (L mg^{-1}) 2.326×10^{-5}	q_0 (mg g^{-1}) 50	R^2 0.998
Freundlich	$\log q_e = \log K_f + \frac{1}{n} \log C_e$	K_f (L mg^{-1}) 0.043	n 1.690	R^2 0.992

the pore geometries entail water zones' minimal resistance to flow. Furthermore, the total water saturation in the porous media, including both water zones and Plateau borders, is associated with capillary pressure. Water is observed to move across the pores to equalize the disparity in capillary pressure [66].

As discussed, surfactant molecules adsorb at the air–water interface. Surfactant molecules form a monolayer at the interface due to this adsorption, which aids in providing an additional mass transfer barrier, reducing foam drainage by migrating surfactant molecules towards foam thinning boundaries (i.e., Marangoni effect) and uniform foam bubble size distribution by lowering surface tension [67]. These processes consecutively reduce the foam coarsening in porous media. Studies have shown that it is exceedingly difficult to maintain foam stability when employing merely surfactant in a severe reservoir environment (i.e., high salinity and temperature) for an extended period [68]. In addition, surfactant adsorption to porous rock surfaces is a significant issue [57]. As a result, many researchers are considering employing nanoparticles as foam stabilizer in addition to the surfactant. Nanoparticles enhance foam stability and reduce excessive surfactant adsorption on porous rock surfaces [69].

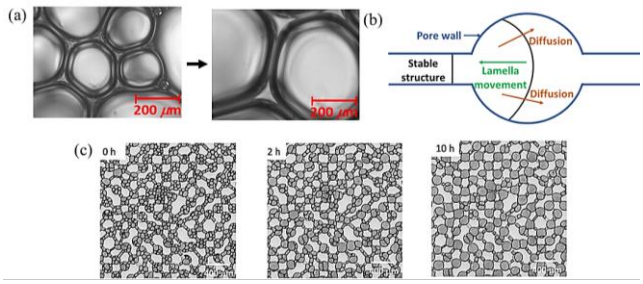

Fig. 8. (a) Small bubbles joining a larger one leads to the foam's coarsening process [Material: 0.25 wt. % sodium dodecyl sulphate solution and instrument: Axiostar, Carl Zeiss], (b) illustration of foam coarsening mechanism, and (c) various microscopic images captured at different time intervals showcasing the foam coarsening process in a pore-scale micromodel [66], reprinted with permission from Frontiers Media S.A., © 2022.

Monitoring the differential pressure across a stacked core assembly in a typical coreflooding experiment allows researchers to examine the stability and performance of foam in porous media flow. Nevertheless, complex foam drainage, coarsening and coalescence mechanisms are highly challenging phenomena to comprehend. Morphological analysis, such as scanning electron microscopy (SEM) and X-ray microcomputed tomography (μCT) are practiced for assessment of pore-scale structures and flow visualization [70]. However, pore-scale micromodels provide an easy, effective, and direct means of visualizing foam coarsening, stability and flow [71]. In Fig. 8(c), the coarsening process of foam in a pore-scale micromodel is depicted at various time intervals (0–10 h) [66]. This visual representation clearly illustrates the gradual merging of smaller bubbles into larger ones as time progresses, ultimately leading to the growth of larger bubbles to the size of a pore.

3.6 Foam quality

Foam quality (f_g) is a measure of the amount of gas in foam, and is calculated as the ratio of the non-wetting (i.e., gaseous) phase velocity (u_g) to the sum of the non-wetting and wetting (i.e., liquid) phases velocity (u_l) (Equation 2) [32].

$$f_g = \frac{u_g}{u_g + u_l} \tag{2}$$

f_g is also a measure of minimum pressure drop and flow velocity required to generate foam in porous media. Depending on the f_g value, foam in porous media can be categorized into three types, *viz*. bubbly liquid (f_g < 64 %), wet foam (64 < f_g < 99 %), and dry foam (f_g > 99 %) [72]. Increasing the f_g value directly impacts both the gas mobility and foam apparent viscosity (μ_{app}^f). As f_g increases, so does the gas mobility and μ_{app}^f. An optimal f_g value is associated with maximum μ_{app}^f. However, μ_{app}^f value falls after the optimal f_g value is passed (see Fig. 9(a)). Furthermore, the trend for ΔP is identical to that of μ_{app}^f (see Fig. 9(b)). Darcy's law can be utilized to determine the μ_{app}^f value in porous media assuming foam as a single fluid phase [72]. As discussed earlier, a significant increase in ΔP across the porous medium indicates generation of foam. Therefore, mobility reduction factor (MRF) is a key parameter for assessing foam performance in porous media [73]. MRF is defined as the ratio between ΔP (with foam) to ΔP (without foam) at steady state condition. Determining the optimal f_g value holds great significance as it directly influences the overall foam performance in porous media [74].

As discussed in Section 3.4, foam has a non-Newtonian (shear-thinning) flow behavior. Further, depending on the f_g its yield-stress values increase (see Fig. 9(c)) [72]. In the high-permeable region of the porous media, the μ_{app}^f increases with f_g. Due to the intricacy of the foam flow in porous media, the foam produced therein exhibits higher rheological properties when compared to bulk foam. However, it becomes challenging to measure the rheological features as f_g rises above the threshold level. The flow behavior of foam fits

well with the Herschel-Bulkley rheological model due to the yield-stress behavior of foam [77].

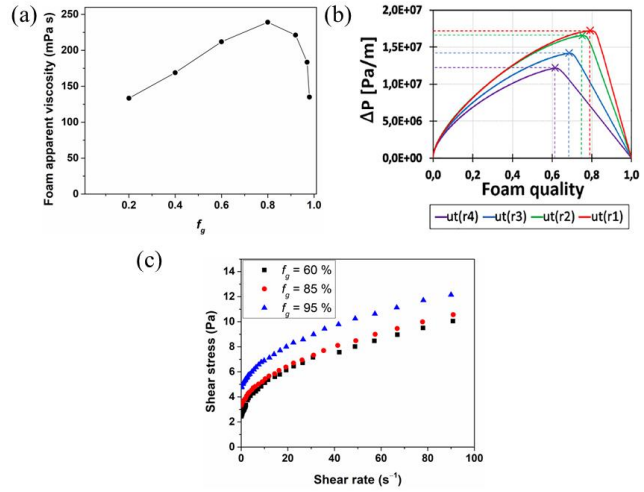

Fig. 9. (a) Foam apparent viscosity (μ_{app}^{f}) as a function of foam quality (f_g) [75], reprinted with permission from American Chemical Society, © 2016, (b) variation in the pressure difference (ΔP) with f_g [76], reprinted with permission from American Chemical Society, © 2022, and (c) foam flow behavior at different f_g [72], reprinted with permission from Elsevier Ltd., © 2020.

3.7 Effective approaches for implementing foam-assisted EOR in reservoir simulation tools

Foam modelling is primarily distinguished into population balance models and the semi-empirical method. Population balance models represent the dynamic processes of generation and degradation, taking into account the impact of bubble size on gas mobility. The semi-empirical method is an implicit method that assumes local equilibrium (LE) between dynamic processes creating and destroying bubbles. The semi-empirical method is widely known as the LE implicit texture model, which implicitly represents the impact foam bubble size through gas mobility reduction factor [78]. One predominant semi-empirical model is that found in STARS and GEM offered by the Computer Modelling Group [79]. Semi-empirical model is function of water saturation, surfactant concentration, limiting capillary pressure, foam dry out, oil composition and salt concentration effect. LE models offer several key benefits. Firstly, they are user-friendly and straightforward to employ. Secondly, they demand fewer parameters compared to other models. Lastly, they avoid certain numerical challenges commonly faced when utilizing population-balance models. The LE models can be exhibited using a function *FM* (foam mobility reduction factor), a product of *F* parameter combinations. These individual *F* parameters capture different physical effects and how they affect the overall foam performance in the porous media. *FM* is defined as follows (see equation 3) [80,81]:

$$FM = \frac{1}{1 + fmmob \cdot F_1 \cdot F_2 \cdot F_3 \cdot F_4 \cdot F_5 \cdot F_6 \cdot F_7 \cdot F_{dry}} \quad (3)$$

Table 2 provides a comprehensive overview of the *F* parameters in equation 3, including their specific details. It also provides details on the controlled parameter, the validity of each *F* parameter, and our recommendations. Numerous studies suggest that the determination of *F* is a critical part [74-76,79]; however, they do not directly indicate the effectiveness of foam in diverting or displacing gas through the reservoir rock. Modifying parameters such as capillary number (*Nc*), oil saturation (*So*), water saturation (*Sw*), and permeability characteristics is typically difficult. Consequently, many studies primarily focus on adjusting the other components of *F* parameters listed in Table 2 (such as *fmcap*, *epcap*, *fmoil*, *epoil*, *fmgcp*, *epgcp*, etc.) in order to achieve the most accurate foam modelling and maximize oil recovery [78,79]. In our view, while these parameters hold physical significance, their specific contributions to the evaluation of foam flow, quality, texture, mobility, and displacement efficiency remain unresolved questions that must be addressed. Moreover, like all fluids, foam also tends to initially occupy regions with high permeability and then transition to regions with lower permeability, which aligns with the principles of percolation theory [82]. However, the precise relationship between these *F* parameters and the flow characteristics of foam still needs to be fully comprehended.

Table 2. Details of *F* parameters [80]

F parameters	Equation	Remarks
fmmob	–	• Indicates mobility reduction factor for the aqueous phase in the presence of foam. • Signifies the maximum ability of the foam to cause a reduction in the gas relative permeability. • Controlling parameters: Type and concentration of chemical additives.
F_1	$F_1 = (C_{surf}/fmsurf)^{epsurf}$ where, C_{surf} = Concentration of surfactant $fmsurf$ = Surfactant concentration at which foam strength becomes unaffected by C_{surf} (generally above CMC) $epsurf$ = exponent which determines the foam stability with respect to C_{surf}	• Indicates how effectively gas bubbles generate in the presence of chemical additives (essentially surfactant). • Controlling parameters: Concentration of surfactant, gas saturation, and the interaction between the gaseous and aqueous phases. • Validity: $0 \leq C_{surf} \leq fmsurf$ • In case the concentration of surfactant used is greater than CMC, F_1 can be considered equal to the unity. • An insight into the adsorption mechanism of chemical additives at the air–water interface is recommended.

		• Determination CMC with surface tension and conductivity measurements is encouraged.
F_2	$F_2 = \left[\frac{fmoil - S_o}{fmoil - floil}\right]^{epoil}$ where, *floil* = Minimum oil saturation which does not impact foam strength. *fmoil* = Critical oil saturation at which foam entirely collapses *epoil* = Exponent which governs foam decay rate due to oil saturation	• Indicates the influence of oil saturation on foam stability. • Controlling parameter: Interaction between chemical additives solution and oil, IFT, and film elasticity. • Validity: $floil < S_o < fmoil$, $F_2 = S_o \leq floil = 1$, and $F_2 = S_o \geq floil = 0$ • An insight into the adsorption mechanism of chemical additives at the oil–water interface is recommended. • Determination of IFT, electrokinetics, and morphological analyses is recommended.
F_3	$F_3 = \left[\frac{fmcap}{N_c}\right]^{epcap}$ where, N_c = Capillary number *fmcap* = Reference-rheology capillary number *epcap* = An exponent	• Function of capillary number and indicates the influence of shear thinning behavior of foam in porous media. • Indicates foam stability in porous media as a function of capillary number (i.e., viscous to capillary forces). • Controlling parameters: shear forces, pressure gradients, fluids injection rates, and foam stability. • Validity: $N_C > fmcap$ and $N_C \leq fmcap = 1$ • If the capillary number is high, foam stability decreases primarily due to the prevalence of shear forces (resulting from increased shear-thinning flow behavior) caused by coalescence, bubble rupture, and drainage. • It is recommended to optimize the f_g and μ_{app}^f values by conducting core flooding experiments. • An understanding of rheological properties of foam using viscometer or rheometer is advised.
F_4	$F_4 = \left[\frac{N_c - fmgcp}{fmgcp}\right]^{epgcp}$ where, *fmgcp* = Reference N_c above which foam can generate	• Indicates role of capillary pressure on foam formation and coarsening in porous media. • Capillary number needs to be determined to identify the point at which foam generation occurs. • Controlling parameters: shear forces, pressure gradients, fluids injection rates, and foam stability. • Validity: $N_C > fmgcp$ and $N_C \leq fmgcp = 0$ • If experiments are carried out at steady state condition (i.e., foam generation and destruction occur at the same time), F_4 can be considered equal to the unity. • Utilizing micromodels is advisable to visualize foam formation and coarsening in porous media.
F_5	$F_5 = \left[\frac{fmomf - X_o}{fmomf}\right]^{epomf}$ where, *fmomf* = critical oil-component mole fraction X_o = oil-component mole fraction	• Indicates foams' dependency to crude oil composition. • Controlling parameters: Oil composition and its physiochemical properties. • Validity: $X_O < fmomf$ and $X_O \geq fmomf = 0$ • A detailed characterization of the oil sample's physicochemical properties and chemical composition is encouraged. • Most researchers do not study the effect of oil composition on foam stability; hence, F_5 can be considered unity.
F_6	$F_6 = \left[\frac{W_s - flsalt}{fmsalt - flsalt}\right]^{epsalt}$ where, W_s = mole fraction of salt component *flsalt* = lower-limit salt-mole-fraction value *fmsalt* = critical saltmole-fraction value *epsalt* = the exponent for the salt-function contribution	• Indicates the impact of salinity on foam stability. • Controlling parameters: Type of chemical additives and their concentration, and composition of brine solution. • A detailed physicochemical characterization (i.e., density, total dissolved solids, and conductivity) as well as compositional characterization of brine solution is recommended. • Determination of foam volume concerning time and salinity can help understand the impact of brine solution on foam stability.
F_7	$F_7 = \left(\frac{1}{fmperm1}\right) \times \left(\frac{perm}{fmperm2}\right) + 1$ where, *fmperm1* = permeability 1 fmperm2 =permeability 2	• Indicates the relationship between foam and permeability. • Foam reduces the effective flow area in the porous media, thus alters the relative permeability characteristics. • Controlling parameters: Water saturation, capillary pressure, f_g , and μ_{app}^f. • A detailed routine and special core analyses are recommended.
F_{dry}	$F_{dry} = 0.5 + \frac{tan^{-1}[epdry(S_w - fmdry)]}{\pi}$ where, *fmdry* = Critical water saturation in which the foam strength changes *epdry* = An exponent for the dry-out contribution	• Indicates variations in foam stability as f_g increases and foam dry-out (i.e., coalesces) by restricting the occurrence of capillary pressure phenomenon. • Controlling parameters: Water saturation, capillary pressure, relative permeability (gas and water), f_g , and μ_{app}^f

4 Summary and recommendations

Foam-assisted EOR is gaining attention because of its ability to reduce gas mobility and create a substantial pressure drop as it flows through porous media. Moreover, it also aids in accessing the low permeable zone in the reservoir by enabling fluid diversion from high permeability zones. However, the complexity of the foam-assisted EOR approach should be understood. Significant challenges include establishing good foam mobility and retaining foam stability over an extended period. Therefore, in the present study, we firmly emphasize analyzing the assessment of interfacial and rheological properties, adsorption, and surface charges. These comprehensive analyses aim to enhance our understanding of foam stability and the development of a stable thin film resulting from the interaction between chemical additives and polar components of crude oil. By gaining insights into interfacial phenomena, we aim to facilitate the design of more effective injection strategies for oil recovery.

Numerous studies have affirmed that the investigation of foam flow and its stability in porous media can be accomplished by analyzing factors such as pressure difference, foam apparent viscosity, and foam quality. Additionally, visualizing the foam flow can be achieved through various morphological analyses. These studies have unveiled several significant advancements and unresolved aspects in comprehending the foam-assisted EOR application. However, we firmly believe there is a greater need for a comprehensive understanding of modelling foam using reservoir simulation tools (for example, CMG-STARS®). It would be far more beneficial to grasp their actual physical and chemical implications and then adjust the modelling parameters appropriately. This approach would make much more sense rather than solely relying on mathematical manipulations of the regulatory modelling parameters.

Acknowledgments

This project was supported with funding from Natural Resources Canada's Emissions Reduction Fund, Offshore research and development program, which is managed and administered by Energy Research and Innovation (Newfoundland and Labrador). We would like to thank and show our appreciation to the Hibernia Management and Development Company (HMDC), Chevron Canada Ltd., Mitacs, and Cnergreen for financial support.

References

1 P. Druetta, P. Raffa, and F. Picchioni, Appl. Energy **252**, 113480 (2019).
2 J. Machale, S. K. Majumder, P. Ghosh, and T. K. Sen, Rev. Chem. Eng. **36**, 789–830 (2020).
3 J. Sheng, *Modern chemical enhanced oil recovery: Theory and practice*. (Gulf Professional Publishing, Massachusetts, USA, 2010).
4 A. Kovscek, J. Pet. Sci. Eng. **98**, 130–143 (2012).
5 N. Kumar, M. A. Sampaio, K. Ojha, H. Hoteit, and A. Mandal, Fuel **330**, 125633 (2022).
6 S. Afzali, N. Rezaei, and S. Zendehboudi, Fuel **227**, 218–246 (2018).
7 S. A. Farzaneh and M. Sohrabi, presented at the EAGE Annual Conference and Exhibition Incorporating SPE Europec, London, UK, 2013.
8 T. Majeed, M. S. Kamal, X. Zhou, and T. Solling, Energy Fuels **35**, 5594–5612 (2021).
9 A. Telmadarreie and J. J. Trivedi, Energies **13**, 5735 (2020).
10 I. Cantat, S. Cohen-Addad, F. Elias, F. Graner, R. Höhler, O. Pitois, F. Rouyer, and A. Saint-Jalmes, *Foams: Structure and dynamics*. (Oxford University Press, Oxford, UK, 2013).
11 P. Ghosh, *Colloid and interface science*. (PHI Learning, New Delhi, India, 2009).
12 J. J. Sheng, *Enhanced oil recovery field case studies*. (Elsevier, Massachusetts, USA, 2013).
13 X. Zhao, Y. Feng, G. Liao, and W. Liu, J. Colloid Interface Sci. **578**, 629–640 (2020).
14 S. H. Talebian, R. Masoudi, I. M. Tan, and P. L. J. Zitha, J. Pet. Sci. Eng. **120**, 202–215 (2014).
15 S. Xiao, Y. Zeng, E. D. Vavra, P. He, M. Puerto, G. J. Hirasaki, and S. L. Biswal, Langmuir **34**, 739–749 (2018).
16 N. Churaev, Adv. Colloid Interface Sci. **104**, XV–XX (2003).
17 A. Isah, M. Arif, A. Hassan, M. Mahmoud, and S. Iglauer, Energy Rep. **8**, 6355–6395 (2022).
18 B. Yadali Jamaloei and R. Kharrat, Transp. Porous Media **81**, 1–19 (2010).
19 M. Al-Shargabi, S. Davoodi, D. A. Wood, V. S. Rukavishnikov, and K. M. Minaev, ACS Omega **7**, 9984–9994 (2022).
20 O. Massarweh and A. S. Abushaikha, Petroleum **8**, 291–317 (2022).
21 K. Ahmadi, D. A. Akrong, E. A. Sripal, F. Sahari Moghaddam, E. K. Ovwigho, C. Esene, J. Machale, A. Telmadarreie, and L. A. James, presented at the Offshore Technology Conference, Houston, USA, 2023.
22 H. R. Afifi, S. Mohammadi, S. Moradi, E. Hamed Mahvelati, F. Mahmoudi Alemi, and O. Ghanbarpour, J. Dispersion Sci. Technol. **44**, 819–830 (2023).
23 H. Jiang, W. Kang, X. Li, L. Peng, H. Yang, Z. Li, J. Wang, W. Li, Z. Gao, and S. Turtabayev, J. Mol. Liq. **337**, 116609 (2021).
24 T. F. Tadros, in *Handbook of Colloid and Interface Science* (de Gruyter, Berlin, Germany 2017).
25 V. Bergeron, J Phys: Condens Matter **11**, R215 (1999).
26 N. Churaev, Adv. Colloid Interface Sci. **104**, XV–XX (2003).
27 L. Wang and R.-H. Yoon, Int. J. Miner. Process **85**, 101–110 (2008).
28 O. A. Falode and O. Ojumoola, J. Pet. Gas Eng. **6**, 22–37 (2015).
29 H. Hematpur, S. M. Mahmood, N. H. Nasr, and K. A. Elraies, J. Nat. Gas Sci. Eng. **53**, 163–180 (2018).
30 M. Sagir, M. Mushtaq, M. Tahir, M. Tahir, and A. Shaik, in *Surfactants for Enhanced Oil Recovery*

Applications (Springer, Cham, Switzerland, 2020), pp. 41–63.
31 P. Johnson, V. Starov, and A. Trybala, Curr. Opin. Colloid Interface Sci. **58**, 101555 (2022).
32 K. Z. Abdelgawad, A. R. Adebayo, A. Isah, and N. S. Muhammed, J. Pet. Sci. Eng. **211**, 110195 (2022).
33 E. Vavra, M. Puerto, S. L. Biswal, and G. J. Hirasaki, Sci. Rep. **10**, 12930 (2020).
34 J. Machale, S. K. Majumder, P. Ghosh, and T. K. Sen, Fuel **257**, 116067 (2019).
35 J. Machale, S. K. Majumder, P. Ghosh, T. K. Sen, and A. Saeedi, Chem. Eng. Commun. (2023). Doi: 10.1080/00986445.2023.2196415
36 C.-H. Chang and E. I. Franses, Colloids Surf., A **100**, 1–45 (1995).
37 M. H. Amaral, J. das Neves, Â. Z. Oliveira, and M. F. Bahia, J. Surfactants Deterg. **11**, 275–278 (2008).
38 S. Samanta and P. Ghosh, Chem. Eng. Res. Des. **89**, 2344–2355 (2011).
39 Q. Sun, Z. Li, J. Wang, S. Li, B. Li, L. Jiang, H. Wang, Q. Lü, C. Zhang, and W. Liu, Colloids Surf., A **471**, 54–64 (2015).
40 Y. Wang, X. Liu, T. Jiao, and J. Niu, J. Surfactants Deterg. **20**, 183–191 (2017).
41 S. Ahmed, K. A. Elraies, I. M. Tan, and M. R. Hashmet, J. Pet. Sci. Eng. **157**, 971–979 (2017).
42 D.-m. Wang, D.-k. Han, G.-l. Xu, and Y. Li, Pet. Explor. Dev. **35**, 335–338 (2008).
43 P. Wei, K. Guo, and Y. Xie, J. Pet. Sci. Eng. **195**, 107597 (2020).
44 M. R. Behera, S. R. Varade, P. Ghosh, P. Paul, and A. S. Negi, Ind. Eng. Chem. Res. **53**, 18497–18507 (2014).
45 A. Telmadarreie and J. J. Trivedi, Colloids Interfaces **2**, 38 (2018).
46 C. Fu and N. Liu, Energy Fuels **34**, 13707–13716 (2020).
47 Y. Wang, Y. Zhang, Y. Liu, L. Zhang, S. Ren, J. Lu, X. Wang, and N. Fan, J. Pet. Sci. Eng. **154**, 234-243 (2017).
48 D. Möbius, R. Miller, and V. B. Fainerman, *Surfactants: Chemistry, interfacial properties, applications*. (Elsevier, Amsterdam, Netherlands, 2001).
49 M. J. Rosen and J. T. Kunjappu, *Surfactants and interfacial phenomena*. (John Wiley & Sons, 2012).
50 J. Machale, D. Al-Bayati, M. Almobarak, M. Ghasemi, A. Saeedi, T. K. Sen, S. K. Majumder, and P. Ghosh, Energy Fuels **35**, 4823–4834 (2021).
51 S. J. Park, J. H. Won, J.-C. Lim, J. H. Kim, and S. Park, J. Ind. Eng. Chem. **11**, 20–26 (2005).
52 M. M. Abdulredha, H. S. Aslina, and C. A. Luqman, Arabian J. Chem. **13**, 3403–3428 (2020).
53 C. T. Q. Dang, Z. J. Chen, N. T. B. Nguyen, W. Bae, and T. H. Phung, presented at the SPE Asia Pacific Oil and Gas Conference and Exhibition, Jakarta, Indonesia, 2011.
54 A. A. Olajire, Energy **77**, 963–982 (2014).
55 M. A. Ahmadi, S. Zendehboudi, A. Shafiei, and L. James, Ind. Eng. Chem. Res. **51**, 9894–9905 (2012).
56 M. S. Mohd Musa, P. Y. Gopalan, N. Yekeen, and A. Al-Yaseri, ACS Omega **8**, 13118–13130 (2023).
57 A. F. Belhaj, K. A. Elraies, S. M. Mahmood, N. N. Zulkifli, S. Akbari, and O. S. Hussien, J. Pet. Explor. Prod. Technol. **10**, 125–137 (2020).
58 J. Machale, S. K. Majumder, P. Ghosh, T. K. Sen, and A. Saeedi, Chem. Eng. Commun. **209**, 143–157 (2022).
59 C. W. Macosko, *Rheology: Principles, measurements, and applications*. (Wiley, New Jersey, USA, 1996).
60 B. Vishal and P. Ghosh, J. Dispersion Sci. Technol. **40**, 206–218 (2019).
61 R. G. Larson, *The structure and rheology of complex fluids*. (Oxford University Press New York, USA, 1999).
62 B. Vishal, Rev. Chem. Eng. **39**, 271–295 (2023).
63 K. Li, M. Sharifnik, K.-H. A. Wolf, and W. R. Rossen, Colloids Surf., A **631**, 127666 (2021).
64 S. Jones, N. Getrouw, and S. Vincent-Bonnieu, Soft Matter **14**, 3490–3496 (2018).
65 W. Yu and M. Y. Kanj, J. Pet. Sci. Eng. **208**, 109698 (2022).
66 W. Yu and X. Zhou, Frontiers Energy Res. **10** (2022).
67 Z. Briceño-Ahumada and D. Langevin, Adv. Colloid Interface Sci. **244**, 124–131 (2017).
68 L. Zhang, G. Jian, M. Puerto, X. Wang, Z. Chen, C. Da, K. Johnston, G. Hirasaki, and S. L. Biswal, Energy Fuels **34**, 15727–15735 (2020).
69 C. Negin, S. Ali, and Q. Xie, Petroleum **2**, 324–333 (2016).
70 K. Li, K.-H. A. Wolf, and W. R. Rossen, Colloids Surf., A **632**, 127800 (2022).
71 W. Yang, J. Lu, B. Wei, H. Yu, and T. Liang, ACS Omega **6**, 6064–6069 (2021).
72 S. Omirbekov, H. Davarzani, S. Colombano, and A. Ahmadi-Senichault, Adv. Water Resour. **146**, 103761 (2020).
73 M. Khajehpour, S. Reza Etminan, J. Goldman, F. Wassmuth, and S. Bryant, SPE J. **23**, 2232–2242 (2018).
74 K. Ma, J. L. Lopez-Salinas, M. C. Puerto, C. A. Miller, S. L. Biswal, and G. J. Hirasaki, Energy Fuels **27**, 2363–2375 (2013).
75 Y. Zeng, A. Muthuswamy, K. Ma, L. Wang, R. Farajzadeh, M. Puerto, S. Vincent-Bonnieu, A. A. Eftekhari, Y. Wang, and C. Da, Ind. Eng. Chem. Res. **55**, 7819–7829 (2016).
76 A. Vicard, O. Atteia, H. Bertin, and J. Lachaud, ACS Omega **7**, 16866–16876 (2022).
77 M. J. Shojaei, A. R. De Castro, Y. Méheust, and N. Shokri, J. Colloid Interface Sci. **552**, 464–475 (2019).
78 A. Saeibehrouzi, M. Khosravi, and B. Rostami, Nat. Resour. Res. **29**, 3363–3384 (2020).
79 L. Ding, L. Cui, S. Jouenne, O. Gharbi, M. Pal, H. Bertin, M. A. Rahman, C. Romero, and D. Guérillot, ACS Omega **5**, 23437–23449 (2020).
80 Computer Modeling Group, STARS™ User's Guide (2021).

81 M. Abbaszadeh, A. Varavei, F. R. Garza, A. E. Pino, J. L. Salinas, M. C. Puerto, G. J. Hirasaki, and C. A. Miller, SPE Reservoir Eval. Eng. **21**, 344–363 (2018).

82 G. Yu and W. Rossen, J. Pet. Sci. Eng. **214**, 110406 (2022).